Journal of Cleaner Production 503 (2025) 145424

Contents lists available at ScienceDirect

Journal of Cleaner Production

journal homepage: www.elsevier.com/locate/jclepro

Resource recovery from acid mine drainage using dispersed alkaline substrate: A geochemical assessment

Rafael León *, Francisco Macías, Carlos R. Cánovas, Ainara Rodrigo, José Miguel Nieto

Department of Earth Sciences & Research Center on Natural Resources, Health and the Environment, University of Huelva, Campus 'El Carmen', Huelva, 21071, Spain

ARTICLE INFO

Handling editor: Tomas B. Ramos

Keywords:
Passive treatment
Iberian pyrite belt
Critical raw materials
Valorization
AMD

ABSTRACT

Acid mine drainage is a global environmental problem due to the release of acid and metal(loid)s into surrounding waters, requiring treatment. However, these leachates also represent an important opportunity for waste valorization, as many of the metals they contain are of economic interest and could be retained in the treatment residues. This study focuses on the geochemical features of precipitates from a Dispersed Alkaline Substrate passive remediation system located at the Esperanza mine, as a first step in assessing the valorization potential. The geochemical profile of the precipitates was analyzed using X-ray diffraction, scanning electron microscope and inductively coupled plasma techniques. The findings reveal preferential fronts of precipitation and the concentration of elements, including Fe, Al, Cu, Zn, and rare earth elements across the profile. These fronts correspond to the dissolution of the alkaline reagent, calcite, and the consequent precipitation of sulfate mineral phases. Correlation analyses showed patterns of co-precipitation among elements, especially concerning fronts of Fe oxyhydroxysulfates, basaluminite, and the varying behaviour of Zn and Rare earth elements. The economic assessment revealed significant concentrations of economically valuable elements within specific depth intervals (i.e. Al: 4.3 tons, Zn: 670 kg, Cu: 370 kg, REE: 35 kg, Co: 16 kg, Y: 1 kg, or Sc: 0.6 kg), indicating areas with substantial potential for element recovery. While the value of the waste ($24,000) from passive treatment may not match that of active mining, its revaluation could help reduce the environmental impact of Acid Mine Drainage by partially offsetting the maintenance costs of passive treatment plants.

1. Introduction

Water resources surrounding mining areas, particularly historical sulfide mine sites, with inadequate or minimal waste management practices, may be severely polluted by acidic leachates, with high concentrations of sulfate and metal(loid)s. These leachates, known as Acid Mine Drainage (AMD), are generated when sulfides are exposed to oxygen, water, and microorganisms (Nordstrom, 1982; Moses et al., 1987). The AMD generation process may persist for decades to centuries in coal mining and up to hundreds to thousands of years in sulfide mining after the cessation of mining activity (Young, 1997; Macías et al., 2017b; Tabelin et al., 2022), eliciting significant global concern (Akcil and Koldas, 2006). The treatment of leachates can be either active or passive. Active treatment involves a continuous expenditure of energy and reagents, while passive systems uses energy sources available in nature (e.g., sun energy, gravity) and requires less maintenance (Johnson and Hallberg, 2005). Passive treatment technology is more suitable for abandoned mining areas where AMD is continuously generated but may lose effectiveness when treating highly acidic and metallic waters due to the precipitation of Fe and Al-rich phases (Ayora et al., 2013). To address these technical issues, the Dispersed Alkaline Substrate (DAS) passive treatment technology has been developed in the last decade. DAS employs an alkaline reagent and inert material mixture that offers porosity and has successfully decreased metallic loads and extreme acidity in AMD, as demonstrated by Caraballo et al. (2009, 2011) and Macías et al. (2012a,b). This technology has been successfully applied in different countries worldwide such as Canada, Ecuador, Spain, or United Kingdom (Rakotonimaro et al., 2016; Delgado et al., 2019; Orden et al., 2021; Millán-Becerro et al., 2023).

In addition to the high levels of contaminants found in AMD, significant concentrations of valuable elements such as Cu, Zn, Ni, Co, and rare earth elements (REE) are also present (León et al., 2021). These elements have been extensively studied for their potential economic value in recent years (e.g., Kefeni et al., 2017; Rakotonimaro et al., 2017; Mwewa et al., 2022; Julapong et al., 2023), as it could lead to more sustainable mining practices globally and help to address one of

* Corresponding author.
E-mail address: Rafael.leon@dct.uhu.es (R. León).

https://doi.org/10.1016/j.jclepro.2025.145424
Received 11 October 2024; Received in revised form 24 February 2025; Accepted 30 March 2025
Available online 1 April 2025

the main challenges facing the modern mining industry - namely, the recycling or repurposing of mining wastes (Lottermoser, 2011). The recovery of base, industrial, and technological metals from AMD treatment wastes can be a valuable resource, particularly for countries without primary extraction capabilities reliant on external sources (Silberglitt et al., 2013).

During the treatment of AMD these economically valuable elements may be preferentially retained due to the selective precipitation of specific elements as the pH increases. In this regard, at low pH in such systems, schwertmannite tends to precipitate, retaining Fe, As, or V, while elements of interest such as Cu or REE are separated from these, which are associated with the precipitation of Al phases at slightly higher pH (Ayora et al., 2016). At Esperanza Mine, a DAS treatment plant operated continuously for 28 months, handling an average input flow of 0.8 L/s of AMD led to the accumulation of elements of economic interest in the treatment wastes, around 32 t of Fe, 6.1 t of Al, 0.8 t of Cu, 0.8 t of Zn, 39.4 kg of REE, 20 kg of Co or 1 kg of Sc according to estimates made from the difference in concentration between the AMD of input and the result of its treatment (Orden et al., 2021). However, a deeper knowledge about the geochemical factors controlling the mobility and fate of these elements during the treatment is needed. Therefore, the main objective of this study is to conduct a direct analysis of the mineralogy and geochemistry of the precipitate profile of the treatment plant to evaluate the behavior of various elements and potential waste valorization opportunities.

2. Study site

The Esperanza mine's treatment facility incorporates a passive DAS-type system, which consists of mixing inert material with an alkaline reagent, in this case limestone. The initial stage of this plant is the Natural Ferroxidizing Lagoon (NFOL), as a pretreatment, which includes a chain of aeration cascades followed by a 100 m^2 settling pond. The purpose of the NFOL stage is to facilitate Fe(II) oxidation and to a lower extent precipitation of iron mineral phases, primarily as schwertmannite (Macias et al., 2012a). The first step is connected to a reagent tank of 960 m^3, divided into two vessels, via open channels. This reactive tank consists of a 0.5 m thick layer of quartz gravel for drainage, a DAS-Limestone reactive layer made up of 80 % pine wood chips and 20 % limestone sand (v/v), and approximately 1.5 m of water supernatant from the base to the upper area. The water processed in the reactive tank circulates to a 100 m^2 settling pond, which enhances the sedimentation of precipitated minerals. After passing through the first reagent tank, the water is subjected to a second set of treatment. This involves another reagent tank of shorter length, resulting in a volume of 720 m^3. The water then proceeds to a second decanter, which is identical to the first one. Finally, the treated water is discharged back into the surrounding water body.

During the operational period of the treatment plant, which was active from December 2014 to April 2017, approximately 56,000 m^3 of AMD were treated until the depletion of the alkaline reagent inside the first tank. The average pH of the AMD from Mina Esperanza is 2.8, with an EC of 2.8 mS/cm and an ORP of 541 mV. Additionally, the AMD exhibited elevated concentrations of various elements, including SO_4 (2872 mg/L), Fe (683 mg/L), Al (117 mg/L), Zn (15 mg/L), Cu (14 mg/L), REE (0.8 mg/L), and As (0.3 mg/L), among others (Orden et al., 2021). This AMD flows from the gallery of an abandoned mine, situated within felsic volcanic rocks, which was operational between 1906 and 1931. During this period, 1.8 million tonnes of polymetallic sulphide (predominantly pyrite and chalcopyrite) were extracted, with a Cu grade between 1 and 2 % (Pinedo Vara, 1963). The treatment of this AMD resulted in the removal of a significant quantity of elements of economic value from the water, including 6.1 tons of Al, 0.8 tons of Cu, 0.8 tons of Zn, 39.4 kg of REE, 20 kg of Co, or 1 kg of Sc. Most of these elements were retained in the first reactive tank (Orden et al., 2021). A detailed view of the mine gallery, the different components of the treatment plant, and the sampling point for the precipitate profile can be accessed via the KML file (Google Earth™), which is provided as an electronic supplement (KML S1).

3. Materials and methods

As stated previously, this study focused on the waste produced at the DAS treatment plant in Esperanza mine after the plant lost efficiency. To collect samples of the precipitates, the inflow of water into the first tank was halted, and a 2 m trench was excavated in its center. Samples were collected in Ziploc© bags at 10 cm intervals along the waste profile (a total of 19 samples) and transported to the laboratory for oven drying at 35 °C for 48 h. Meanwhile, a portion of each residue sample was chosen through quartering and powdered in a ring mill. The aqua regia method was employed to digest the powdered residue using 12 M HCl with 37 % purity and 15.8 M HNO_3 with 65 % purity at a 3:1 ratio. The major and trace element content in wastes was analyzed by Inductively Coupled Plasma-Atomic Emission Spectroscopy (ICP-AES) and Inductively Coupled Plasma-Mass Spectroscopy (ICP-MS) at the Central Research Services of the University of Huelva. The detection limits for major elements were as follows: 0.2 mg/L for Al, Cu, Mg, and Zn, 0.1 mg/L for Fe and Mn, and 0.5 mg/L for S. For trace elements, the detection limit was 2 μg/L. A portion of the powdered samples was subjected to mineralogical analysis through X-ray diffraction (XRD) with Cu Kα radiation using a Bruker D8 Advance X-ray diffractometer, and through a JEOL JSM-IT500HR Field Emission Scanning Electron Microscope coupled with Oxford Xmax 150 Energy Dispersive System (FESEM-EDS). To quantify the mineralogical composition of the samples, the percentage of each mineral (by weight) was determined through a semi-quantitative mineralogical analysis of the crystalline phases from the XRD spectrum, employing the XPowder code (Martin, 2004).

The metallic content of the waste was determined by calculating the concentration of each element and the density of the samples. The waste's density was estimated by measuring the weight of a known volume of the waste every 10 cm using a precision balance. To determine the commercial value of the waste, various sources to gather the market prices of each metal were accessed (i.e., ISE, 2023; LME, 2023; SMM, 2023; USGS, 2023).

Subsequently, the ratios between the light (LREE; La to Sm), middle (MREE; Eu to Dy), and heavy REE (HREE; Ho to Lu), as $(HREE/LREE)_{NASC}$, $(MREE/LREE)_{NASC}$, and $(HREE/MREE)_{NASC}$, using the method of Stolpe et al. (2013), averaging all possible permutations of inter-element ratios. Furthermore, the Eu anomaly (Eu^*_N) was calculated using the interpolation of nearby normalized rare earth element values, as described by the equation (Noack et al., 2014):

$$Eu^*_N = 2[Eu]_N \ / \ ([Sm]_N + [Gd]_N)$$

The Pearson correlation matrix was employed to analyze the correlations between elements. While some elements, such as Fe, Al, and other associated elements (Figs. 3 and 4), exhibit asymmetric distributions, a considerable number of the elements of interest (i.e., REE, Zn, and other related elements) display normal distributions (Figs. 5 and 6).

4. Results and discussion

4.1. Controlling factors and mineralogical dynamics in precipitation profiles: insights from XRD and geochemical analyses

The XRD results show that the composition of the precipitate profile can be partly controlled by dissolution-precipitation reactions of main minerals (Fig. 1). It is worth noting that calcite is the primary reagent used to treat acidic water, and its abundance through the waste profile is related to the incomplete dissolution and/or coating of this mineral during the treatment. Consequently, its dissolution causes the precipitation of metal(loid)-rich mineral phases. It is evident that within the upper 40 cm of the profile, the proportion of calcite is low due to contact

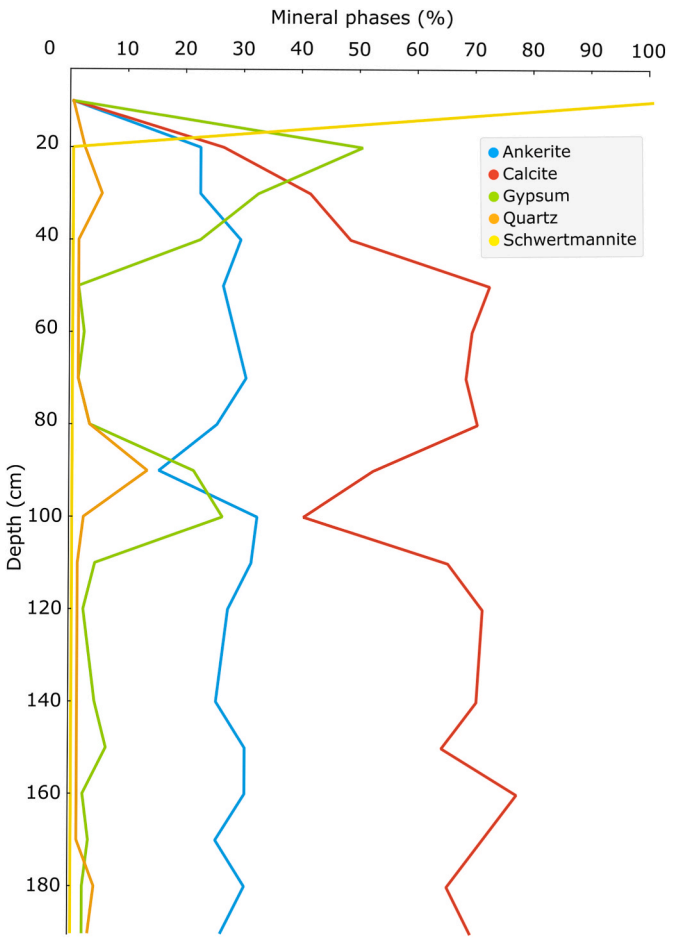

Fig. 1. Percentage of main minerals precipitated in the Esperanza mine reactive tank, detected through XRD. For illustrative purposes, the supplementary material (Fig. S1) includes a selection of XRD spectra.

with more acidic water, which enhances its dissolution. From this initial depth, the proportion of calcite in relation to other minerals remains relatively consistent, averaging approximately 70 %. However, there are areas where this proportion is lower (e.g. at a depth of 100 cm). This is likely due to the presence of preferential channels through which water filters, thereby reducing the homogeneity in the effectiveness of treatment (Fig. 1). As a result of the dissolution of calcite by AMD, a significant Fe precipitation is observed in the tank, mainly as schwertmannite, a Fe oxyhydroxysulfate ($Fe_8O_8(OH)_6(SO_4)\cdot nH_2O$), approaching almost 100 % in the upper 10 cm. From a depth of 20 cm down, the alkaline conditions reached after calcite dissolution leads to the precipitation of the remaining Fe as carbonate, mainly ankerite ($Ca(Fe^{2+},Mg,Mn)(CO_3)_2$). Additionally, there are significant fronts with abundance of gypsum ($CaSO_4\cdot 2H_2O$), precipitated after water supersaturation due to the large amount of dissolve sulfate from the AMD and Ca released by the dissolution of calcite. Finally, quartz is also present along the profile, which is likely due to the existence of silica clasts carried by the AMD flow. A mineral that commonly controls the solubility of elements like Al or Cu in AMD environments is basaluminite (Carrero et al., 2015). Although this mineral was not detected by XRD due to its low crystallinity, geochemical studies using PHREEQC (Orden et al., 2021) and direct observations of the precipitate using a FESEM-EDS demostrated its notable presence (Fig. S2).

Regarding the chemical composition of the waste profile (Fig. 2, Table S1), it becomes evident from Ca and Mg (found in minor quantities in calcite) data the existence of various fronts of preferential dissolution of the reagent. These dissolution fronts can be observed in the upper 40 cm and at depths ranging between 80-100 and 130–150 cm (Fig. 2A). After calcite dissolution the pH on these fronts increases, leading to precipitation of most of the metals in the water, primarily in the form of sulfate and oxyhydroxisulfates. As a result, preferential calcite dissolution fronts coincide with high contents in sulfate (Fig. 2B). The concentration of sulfate is notably elevated within the upper 40 cm, ranging from over 100 g/kg in the upper section to 40 g/kg in the lower one. Consequently, high sulfate contents are also observed in other calcite dissolution fronts, at depths of 70–110 cm and between 130 and 150 cm, with quantities reaching up to 70 and 35 g/kg of sulfate, respectively.

In the upper 10 cm, schwertmannite dominates the mineralogical assemblage (Fig. S2), resulting in a significant concentration of Fe (almost 500 g/kg), which decreases drastically from 20 cm depth (less than 10 g/kg in most samples) (Fig. 2C). This mineral can promote the coprecipitation and adsorption of various other elements, including As (Carrero et al., 2015), whose levels can reach nearly 500 mg/kg in the initial centimeters (Fig. 2C.). This will be further discussed in the following section. Below the upper 10 cm, the precipitation of basaluminite may prevail. The consistent accumulation of Al below this depth, with contents of up to about 60, 50 and 30 g/kg in the 10–40, 80–100 and 130–150 cm deep fronts, respectively, suggests this possibility (Fig. 2D). Significant Cu concentrations are also observed coinciding with these fronts, reaching up to 8.4, 5.2, and 1.3 g/kg, respectively (Fig. 2D). This accumulation could be explained by Cu adsorption and/or coprecipitation in basalaluminite, as reported by Carrero et al. (2015). In this regard, the relationship of both native Cu and Cu sulfide/sulfate minerals with basaluminite has been observed through FESEM images (Fig. S2).

However, certain elements follow a different distribution among the precipitation fronts mentioned above. This is the case for elements like Zn, with concentrations that increase from 20 cm depth down, averaging 2 g/kg, although with a Zn peak between 80 and 90 cm, with contents nearing 4 g/kg (Fig. 2E), and concentrations exceeding 3 g/kg in the last 30 cm. The formation of independent particles comprising Zn and S (Fig. S2) may be the reason behind this phenomenon. REE exhibit a remarkable distribution among the reactive dissolution fronts. The highest concentration of these elements is found below the upper 10 cm of depth (Fig. 2F), coinciding with the first aluminum front. At this layer, LREE, MREE, and HREE are retained at rates of 148, 36, and 20 mg/kg, respectively. Below this layer, REE concentration gradually declines with regular minor peaks that do not match the remaining precipitation zones. This suggests the occurrence of other minor mineral phases which could control REE solubility along the tank. In this sense, the precipitation of carbonates and phosphates have been previously suggested as REE scavengers in AMD treatment system (Edahbi et al., 2018; Hermassi et al., 2022; Kotte-Hewa et al., 2023). Although, REE can replace Ca in the gypsum structure, this mechanism is of minor importance during the treatment of AMD (Kotte-Hewa et al., 2024). The presence of some REE phosphate particles with a composition analogous to monazite has been identified (Fig. S2), which could account for the observed distribution of these elements along the tank profile.

4.2. Element co-precipitation and correlation patterns in precipitation profiles

To examine the relationships and precipitation patterns among various elements, a correlation matrix (Table S2) was performed which evidences the existence of multiple clusters of elements that may co-precipitate on various fronts mentioned earlier.

As previously noted, the precipitation fronts consisting mostly of sulfates and oxyhydroxysufates are linked to the effective dissolution of calcite along the tank. However, it is noteworthy that undissolved calcite or some Fe carbonates also exist as fronts within the tank. In this sense, as shown in Table S2, S is inversely correlated with Ca, Mg and Sr ($R^2 = -0.983$, -0.875, and -0.966, respectively).

On the other hand, Fe exhibits a poor correlation with S ($R^2 = 0.636$),

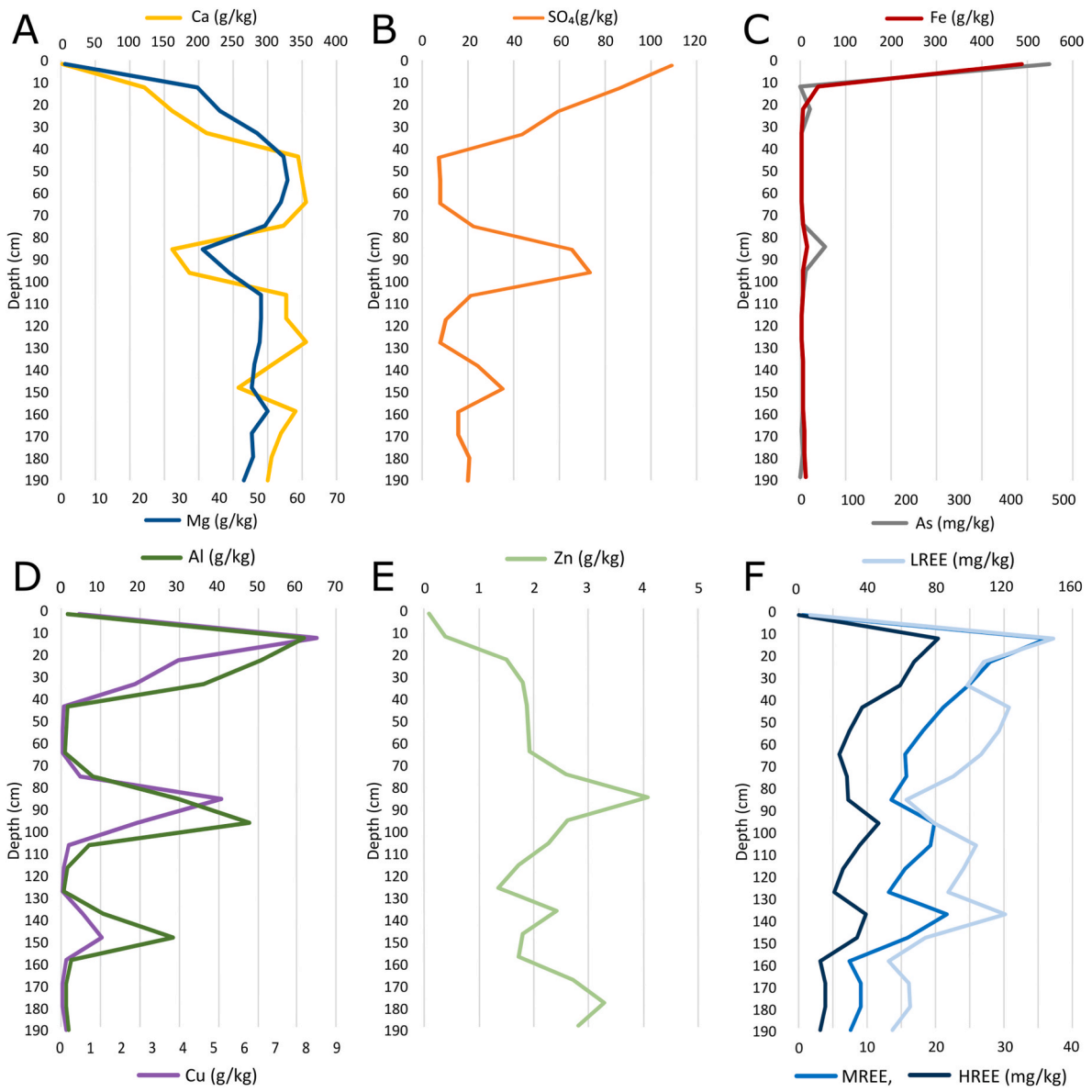

Fig. 2. Concentration profile of the main elements in the Esperanza mine reactive tank.

despite the intense precipitation of Fe oxyhydroxysulfate in the upper 10 cm, because below this depth, the remaining dissolved Fe precipitates as carbonate and other sulfate and oxyhydroxysulfate minerals (e.g., gypsum, basaluminite) precipitate along the profile. In contrast, Fe displays significant correlations with other elements such as As, V and Mo ($R^2 = 0.993$, 0.997, and 0.986 respectively) (Fig. 3; Fig. S3), due to its potential coprecipitation and/or adsorption in schwertmannite (e.g., Carrero et al., 2015; Marouane et al., 2021). Additionally, Fe shows a strong correlation with K ($R^2 = 0.991$), which can be retained during the transformation from schwertmannite to jarosite (Sánchez-España et al., 2012; Jiménez et al., 2023) (Fig. 3). However, this mineral was not identified by XRD probably because the content is below the quantification limit (around 5 %). Additionally, certain elements exhibit their highest concentration in the first 10 cm of the profile, including Na, P, and Sb, exhibiting a notable correlation with Fe ($R^2 = 0.954$, 0.769, and 0.933, respectively) (Table S1). These elements may potentially be retained in schwertmannite or jarosite (Marouane et al., 2021; Jiménez et al., 2023).

As previously stated, sulfate may precipitate predominantly as basaluminite below the upper 10 cm, so the correlation between S and Al is quite high excluding the first sample ($R^2 = 0.953$) (Fig. 4), associated to schwertmannite. In these basalaluminite precipitation zones, additional elements such as Sc or U are preferentially retained (Fig. S4), as evidenced by their significant correlation with Al ($R^2 = 0.985$ and 0.986, respectively) (Fig. 4). Additionally, Cu exhibits a similar trend to that of aluminum zones (Fig. S4), though the different concentration peaks of Cu and Al in the first zone results in a lower correlation between both elements ($R^2 = 0.879$).

Other elements such as Co and Ni seem to have a similar distribution than Zn along the waste profile (Fig. S4). Both elements also exhibit an increase in concentration with depth, with an enrichment front between 70 and 110 cm (Fig. S4). This similar distribution makes that both elements show significant correlations with Zn ($R^2 = 0.884$ and 0.690, respectively) (Fig. 5). It is remarkable the lack of correlation of these elements with Al, unlike other elements preferentially scavenged by basaluminite such as Cu, Sc or U. This poor correlarions are caused by the lack of incorporation of Zn, Co and Ni in all basaluminite fronts (only detected at 70–110 cm). This could be attributed to the pH conditions reached inside the tank, since basaluminite may precipitate at a broad pH range above 4.0, the incorporation of trace elements may be strongly

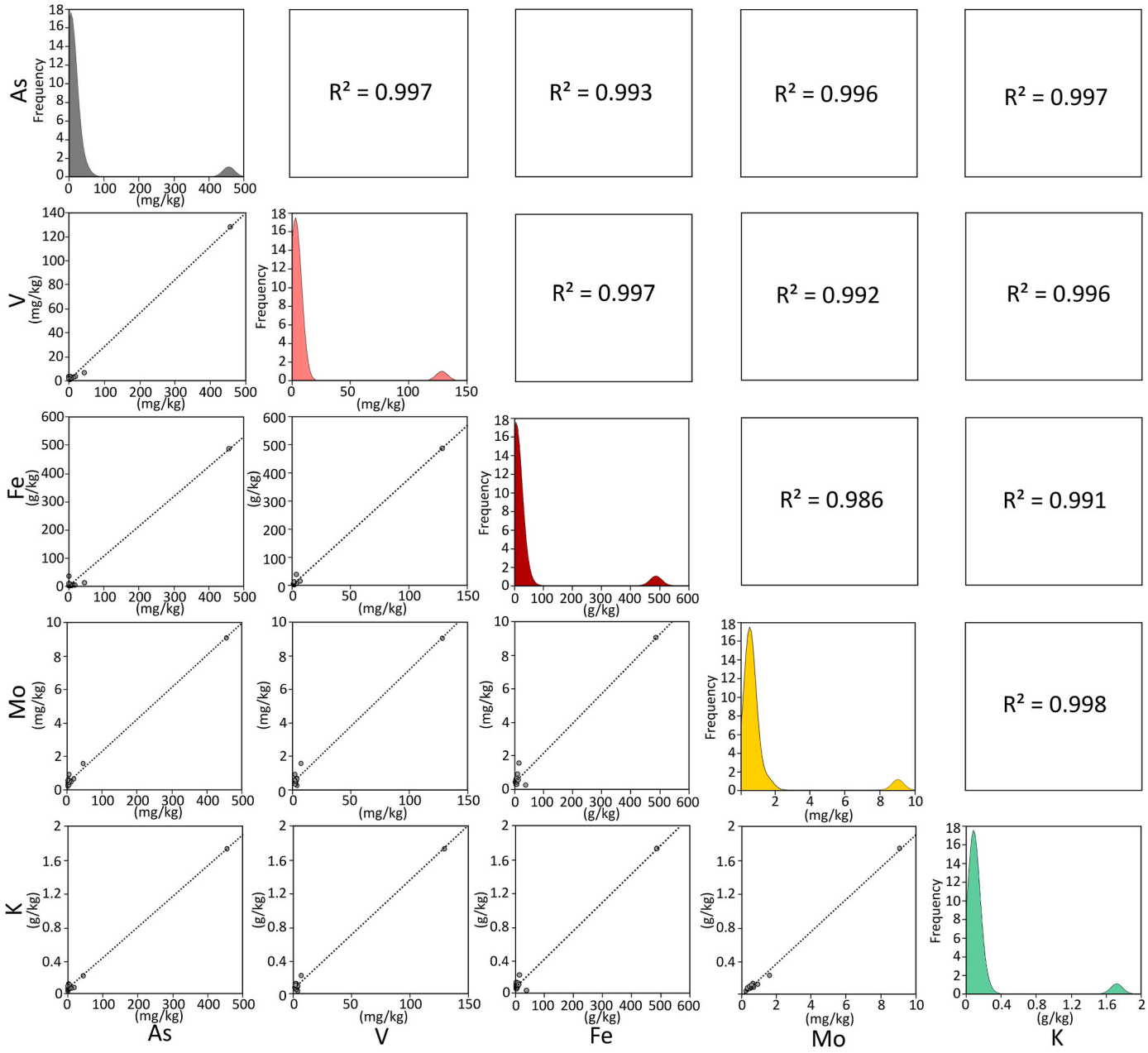

Fig. 3. Scatter plot, concentration histogram, and correlation coefficient analysis of the elements in the Fe precipitation front in the Esperanza mine reactive tank. Fig. S3 presents the concentration profile of these elements.

controlled by medium pH (Lozano et al., 2019). Thus, higher pH values are required for Zn, Co and Ni incorporation into bsaluminite than those required for Cu, Sc or U.

Regarding REE, there exists a significant correlation between these elements, as evidenced by the high R^2 values observed between HREE and MREE (R^2 = 0.970) (Fig. 6), which has been widely reported as these elements have similar geochemical properties. However, the correlation between HREE and MREE in relation to LREE is lower (R^2 = 0.745 and 0.881, respectively) (Fig. 6), possibly due to the preferential precipitation of La and, to a lesser extent, Ce compared to the other REE (Fig. S6), resulting in a particular correlation with the Ca group (R^2 = 0.754 and 0.632 of La vs Ca and Ce vs Mg, respectively) (Table S2). This higher correlation of LREE with Ca have been previously reported (e.g., Ayora et al., 2022; Kotte-Hewa et al., 2024). Moreover, Y, which is commonly associated with REE, shows a strong correlation with this element group (R^2 = 0.852). It has a higher correlation with LREE (R^2 = 0.870) compared to MREE and HREE (R^2 = 0.744 and 0.626, respectively) (Fig. 6). The element that exhibits the strongest correlation with REE is Se, with R^2 values as high as 0.974 and 0.987 compared to HREE and MREE respectively, while showing a somewhat lower correlation with LREE (R^2 = 0.844) (Fig. 6). The association of Se with REE in the wastes generated during the AMD treatment has not been reported before, and requires deeper research. Another element, Ga, displays a precipitation pattern similar to that of REE (Fig. S6), although the correlation is not very high due to some significant differences (R^2 = 0.671, 0.692 and 0.562 with respect to HREE, LREE and MREE, respectively) (Fig. 6). As commented before, REE follows a complex distribution along the tank profile, with elevated contents associated to Fe, Al, and there mineral fronts (e.g., sulfate, carbonate and/or phosphate).

Finally, although there is no strong correlation between the REE contents in the treatment plant profile and the primary Fe or Al fronts along with other elements, a correlation has been noted between specific

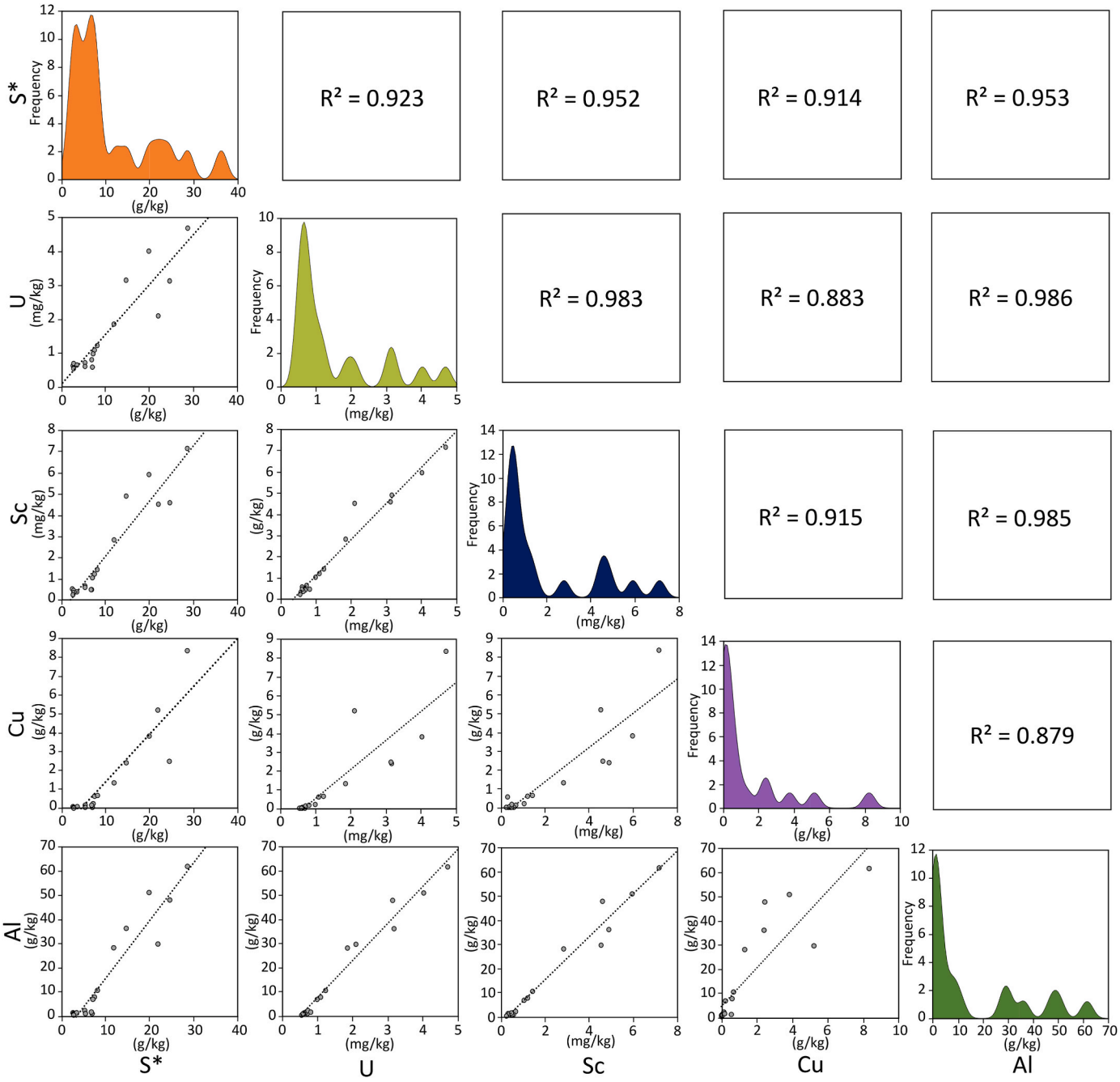

Fig. 4. Scatter plot, concentration histogram, and correlation coefficient analysis of the elements in the Al precipitation fronts in the Esperanza mine reactive tank. Fig. S4 presents the concentration profile of these elements.

parameters or ratios associated with the REE, and these fronts. This concerns the ratios between normalized HREE, MREE, and LREE (HREE/LREE, MREE/LREE, and HREE/LREE), as well as the Eu anomaly (Eu*N), which vary with depth in ways very similar to Cu or Al (Fig. S7, Table S2). This could indicate a REE fractionation during the AMD treatment, with preferential accumulation of MREE and HLREE in the basaluminite fronts, and a preferential accumulation of LREE, including negative Eu anomaly, in other mineral fronts. In this sense, LREE are commonly incorporated in carbonates, phosphates, and gypsum (Kanazawa and Kamitani, 2006; Ayora et al., 2022; Kotte-Hewa et al., 2023).

4.3. Economic assessment of the metal(loid) precipitation profile

The passive AMD treatment plant in Esperanza mine resulted in significant metal(loid) precipitation, some of which possess high economic value and are selectively accumulated on different mineral fronts. To evaluate the scale of economic interest in these secondary mineral deposits, the total mass of each element was computed, considering the analyzed concentration and residue density (Table S3). In Fig. 7, the metal loads retained in the Esperanza mine tank are displayed. Among the majority elements shown in Fig. 7A., the high mass of calcium or magnesium is significant (they can reach up to 7 and 1 ton/10 cm, respectively), which would correspond to the calcite not reacted during the treatment. In addition, a high amount of Fe in the upper 10 cm (10 tons) is also notable, along with other elements of low economic value

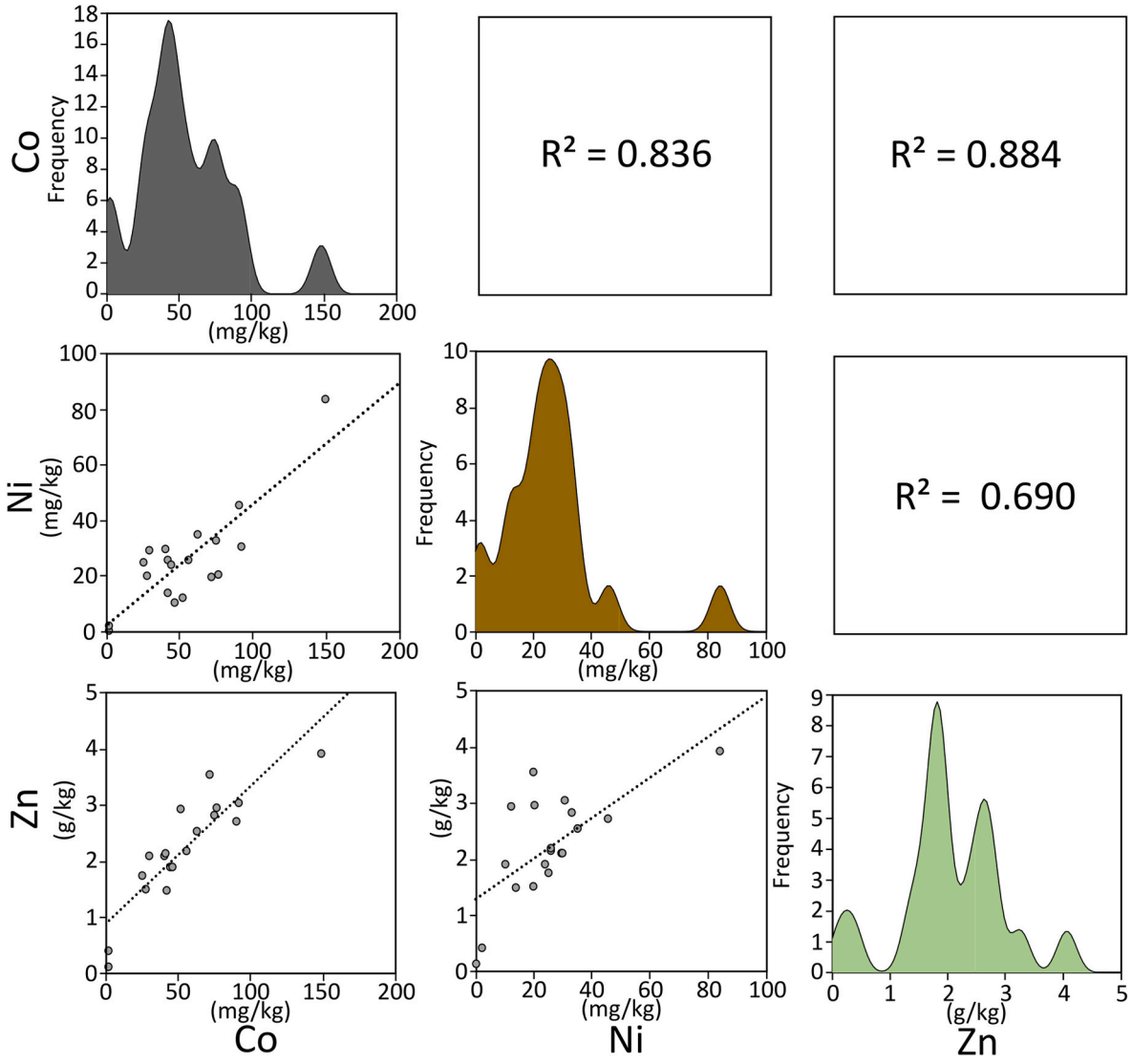

Fig. 5. Scatter plot, concentration histogram, and correlation coefficient analysis of the elements in the Zn precipitation fronts in the Esperanza mine reactive tank. Fig. S5 presents the concentration profile of these elements.

(9.5 kg of As or 2.6 kg of V). There are also significant quantities of S in this first layer (750 kg). Of economic interest are the high amounts of Cu retained in the three main precipitation fronts, up to 130, 50, and 25 kg/10 cm (Fig. 7B), respectively, which coincide with high amounts of Al, up to 900, 600, and 500 kg/10 cm, respectively. Additionally, Zn is distributed more uniformly throughout the profile, ranging between 20 and 50 kg/10 cm (Fig. 7B). Some minor elements in the precipitate exhibit potential economic value, including REE, Co, Y, Ni, or Sc (with quantities up to 3, 1.6, 1, 0.8 or 0.1 kg/10 cm, respectively) (Fig. 7C). Additionally, they appear to be more concentrated in areas where Al-Cu precipitates are lower. Pb is also detectable, which could be of economic interest, although in smaller amounts (0.6 g in the first 10 cm), and mostly concentrated within the first 10 cm together with non-useable elements.

The element distribution along the profile reveals a series of enriched fronts with high economic potential. It should be noted that the upper 10 cm presents a lower value due to the characteristic of the precipitate, which accumulates a significant portion of elements with limited economic interest or elements that impose economic penalties due to their toxicity, including Fe, As, and V. However, just below this front (between 10 and 40 cm depth) a section with significant economic potential is observed (Fig. 7D.). This 30 cm front accumulate metals with a potential value of almost $10,000, equivalent to 42 % of the economic potential of the waste present in the tank, which may amount to $24,000 (Table S4). The second section, which extends from 70 to 110 cm, would contribute 24 % of the total economic potential ($5700), and the third section, found at a depth of 130–150 cm, would represent 15 % ($3600). These high-economic potential fronts overlap with fronts of basaluminite precipitation. Along with Al, whose potential is high due to the substantial quantity that precipitates (over 43 % of the total economic potential), other interesting elements such as Cu and Sc are concentrated (14.1 and 12.6 % of the total economic potential, respectively), as well as some quantities of Zn and REE. The remaining metal concentrate has an average potential value of about $500 per 10 cm thanks to the occurrence of elements such as REE, Zn, Co and Y throughout the profile, which represent remarkable percentages of the total economic potential (15.1, 8.6, 2.3 and 1.6 %, respectively). Elements such as Ni, Ga, Ge, Sn, or Pb that may provide high revenues have concentrations too low to contribute signifciantly to the total economic potential, representing less than 2.5 % of the total.

While the economic potential of this waste is not comparable to that of active mining operations, its revaluation can boost the mitigation of water impact by AMD by partially offsetting costs associated with the maintenance of DAS-type passive treatment plants. This offset is

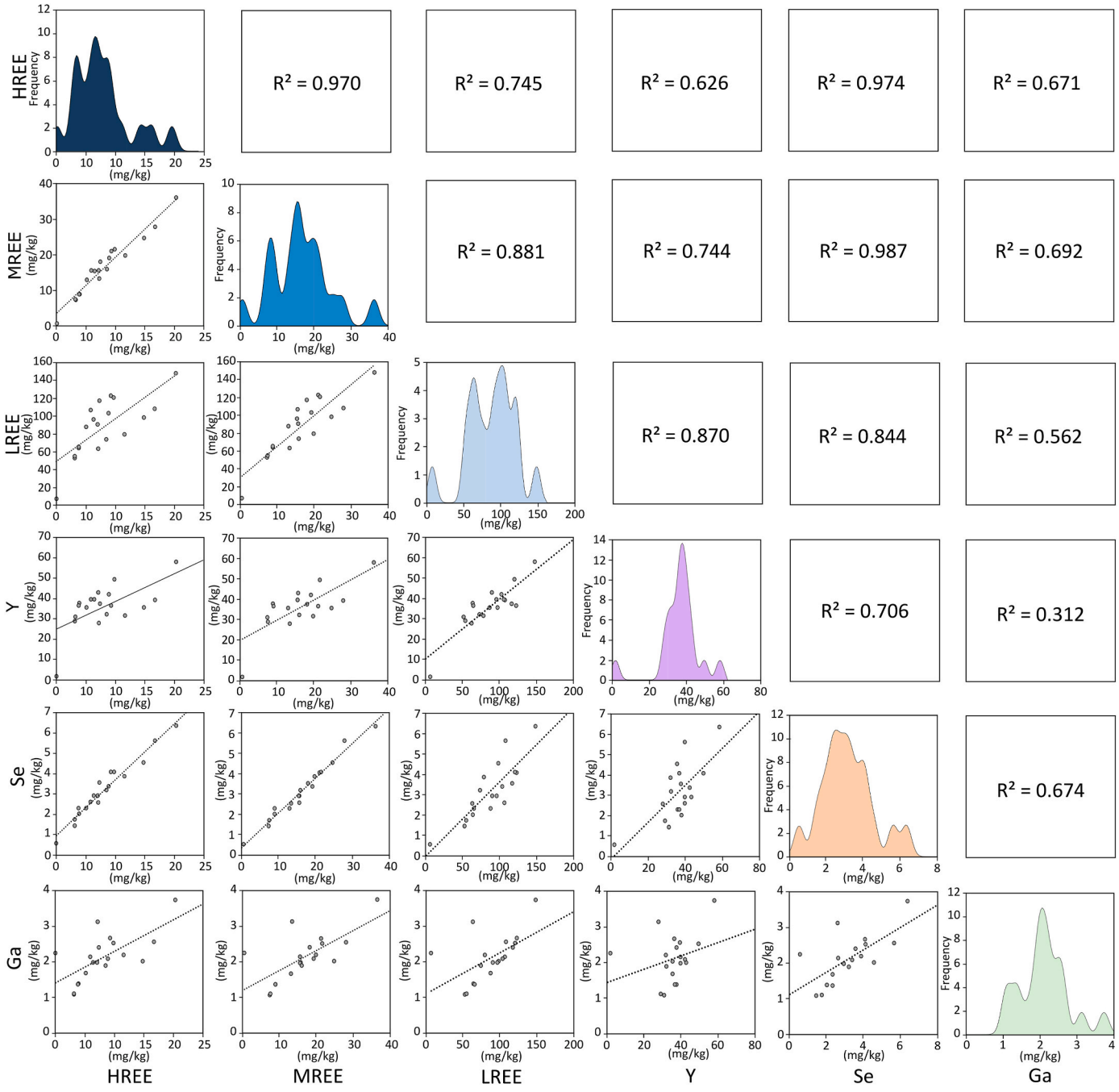

Fig. 6. Scatter plot, concentration histogram, and correlation coefficient analysis of the elements in the REE precipitation fronts in the Esperanza mine reactive tank. Fig. S6 presents the concentration profile of these elements.

estimated at around €8428 annually (Orden et al., 2021). However, it must be highlighted that the real values differ from those estimated in this work, since are based on the total extraction of elements from the waste and the purity of the final product, however, technical limitations usually leads to the reduction of the final revenues which, according to previous experience, could reach up to 70 % (Smith et al., 2013). This is because, although the extraction of metals contained in these wastes is easily and cost-effectively performed (Macías et al., 2017a), the obtaining of a pure product is the limiting factor despite the technological and industrial advances obtained in last years.

5. Conclusions

The geochemical analysis of wastes generated during the operation of the Disperse Alkaline Substrate (DAS) passive treatment plant at Esperanza mine revealed complex patterns of element distribution associated with the geochemical conditions reached during the treatment process. The study showed the importance of dissolution-precipitation reactions of major minerals to control the chemical composition of the precipitate profile. This leads to the selective retention of different elements within specific depth intervals, which is associated with the preferential dissolution of the alkaline reactant in certain zones and the subsequent formation of oxyhydroxisulfate minerals, such as schwertmannite or basaluminite. Areas with high economic potential have been identified due to the correlation of elements including Cu or Sc with the main basaluminite fronts, along with other elements such as Zn, Co, REE, and Y which are spread throughout the profile. Due to the presence of over 4.3 tons of Al, 670 kg of Zn, 370 kg of

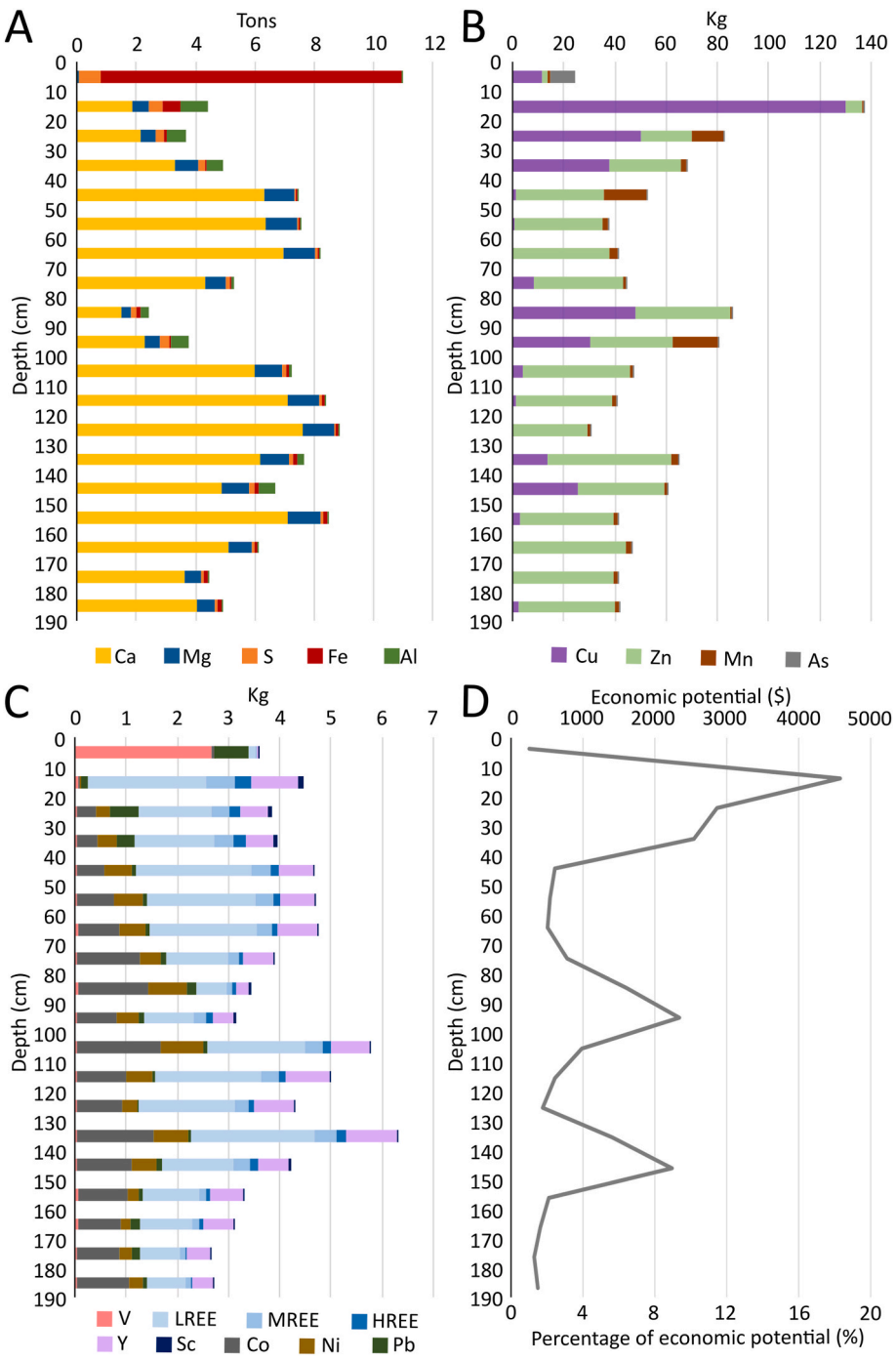

Fig. 7. Weight of the main elements and economic potential (in both total dollar value and percentage of the total) along the precipitation profile in the Esperanza mine reactive tank.

Cu, 35 kg of REE, 16 Kg of Co, 1 Kg of Y, or 0.6 Kg of Sc in the tank, there is an economic potential of up to $24,000. This potential is concentrated mainly in the basaluminite fronts, which accumulate up to 80 % of the total economic potential. While this economic potential cannot be compared to the magnitude generated in active mines, these findings highlight the chance to valorize wastes to mitigate the environmental impacts of acid mine drainage and potentially offset the maintenance costs of passive treatment facilities. Further research into mineralogy and extraction methods has the potential to improve the economic feasibility of recovering valuable elements from acid mine drainage treatment.

CRediT authorship contribution statement

Rafael León: Writing – original draft, Visualization, Investigation, Formal analysis, Data curation. **Francisco Macías:** Writing – review & editing, Supervision, Investigation, Conceptualization. **Carlos R. Cánovas:** Writing – review & editing, Supervision, Funding acquisition. **Ainara Rodrigo:** Writing – review & editing, Investigation. **José Miguel Nieto:** Writing – review & editing, Supervision, Funding acquisition.

Declaration of competing interest

The authors declare that they have no known competing financial

interests or personal relationships that could have appeared to influence the work reported in this paper.

Acknowledgements

This research was supported by ERA-MIN3 SuMRee project (PCI2024-153500), financed by MICIU/AEI/10.13039/501100011033, and by the European Union NextGenerationEU/PRTR. We would also like to thank Editorial Team and anonymous reviewers for the support and suggestions that significantly improved the quality of the original paper.

Appendix A. Supplementary data

Supplementary data associated with this article can be found, in the online version, at https://doi.org/10.1016/j.jclepro.2025.145424.

Data availability

Data will be made available on request.

References

Akcil, A., Koldas, S., 2006. Acid Mine Drainage (AMD): causes, treatment and case studies. J. Clean. Prod. 14 (12–13), 1139–1145. https://doi.org/10.1016/j.jclepro.2004.09.006.

Ayora, C., Caraballo, M.A., Macias, F., Rötting, T.S., Carrera, J., Nieto, J.M., 2013. Acid mine drainage in the Iberian Pyrite Belt: 2. Lessons learned from recent passive remediation experiences. Environ. Sci. Pollut. Control Ser. 20, 7837–7853. https://doi.org/10.1007/s11356-013-1479-2.

Ayora, C., Macías, F., Torres, E., Lozano, A., Carrero, S., Nieto, J.M., et al., 2016. Recovery of rare earth elements and yttrium from passive-remediation systems of acid mine drainage. Environ. Sci. Technol. 50 (15), 8255–8262. https://doi.org/10.1021/acs.est.6b02084.

Ayora, C., Carrero, S., Bellés, J., Basallote, M.D., Cánovas, C.R., Macías, F., 2022. Partition of rare earth elements between sulfate salts formed by the evaporation of acid mine drainage. Mine Water Environ. 41 (1), 42–57. https://doi.org/10.1007/s10230-021-00803-0.

Caraballo, M.A., Rötting, T.S., Macías, F., Nieto, J.M., Ayora, C., 2009. Field multi-step limestone and MgO passive system to treat acid mine drainage with high metal concentrations. Appl. Geochem. 24 (12), 2301–2311. https://doi.org/10.1016/j.apgeochem.2009.09.007.

Caraballo, M.A., Macías, F., Rötting, T.S., Nieto, J.M., Ayora, C., 2011. Long term remediation of highly polluted acid mine drainage: a sustainable approach to restore the environmental quality of the Odiel river basin. Environ. Pollut. 159 (12), 3613–3619. https://doi.org/10.1016/j.envpol.2011.08.003.

Carrero, S., Pérez-López, R., Fernandez-Martinez, A., Cruz-Hernández, P., Ayora, C., Poulain, A., 2015. The potential role of aluminium hydroxysulphates in the removal of contaminants in acid mine drainage. Chem. Geol. 417, 414–423. https://doi.org/10.1016/j.chemgeo.2015.10.020.

Delgado, J., Barba-Brioso, C., Ayala, D., Boski, T., Torres, S., Calderón, E., López, F., 2019. Remediation experiment of Ecuadorian acid mine drainage: geochemical models of dissolved species and secondary minerals saturation. Environ. Sci. Pollut. Control Ser. 26, 34854–34872. https://doi.org/10.1007/s11356-019-06539-3.

Edahbi, M., Plante, B., Benzaazoua, M., Ward, M., Pelletier, M., 2018. Mobility of rare earth elements in mine drainage: influence of iron oxides, carbonates, and phosphates. Chemosphere 199, 647–654. https://doi.org/10.1016/j.chemosphere.2018.02.054.

Hermassi, M., Granados, M., Valderrama, C., Ayora, C., Cortina, J.L., 2022. Recovery of rare earth elements from acidic mine waters: an unknown secondary resource. Sci. Total Environ. 810, 152258. https://doi.org/10.1016/j.scitotenv.2021.152258.

ISE, 2023. Institut für seltene Erden und strategische Metalle. https://institut-selteneerden.de/ (accessed June 2023).

Jiménez, A., Marban, G., Roza-Llera, A., 2023. From schwertmannite to natrojarosite: long-term stability and kinetic approach. Am. Mineral. 108 (1), 150–159. https://doi.org/10.2138/am-2022-8288.

Johnson, D.B., Hallberg, K.B., 2005. Acid mine drainage remediation options: a review. Sci. Total Environ. 338 (1–2), 3–14. https://doi.org/10.1016/j.scitotenv.2004.09.002.

Julapong, P., Numprasanthai, A., Tangwattananukul, L., Juntarasakul, O., Srichonphaisarn, P., Aikawa, K., et al., 2023. Rare earth elements recovery from primary and secondary resources using flotation: a systematic review. Appl. Sci. 13 (14), 8364. https://doi.org/10.3390/app13148364.

Kanazawa, Y., Kamitani, M., 2006. Rare earth minerals and resources in the world. J. Alloys Compd. 408, 1339–1343. https://doi.org/10.1016/j.jallcom.2005.04.033.

Kefeni, K.K., Msagati, T.A., Mamba, B.B., 2017. Acid mine drainage: prevention, treatment options, and resource recovery: a review. J. Clean. Prod. 151, 475–493. https://doi.org/10.1016/j.jclepro.2017.03.082.

Kotte-Hewa, D.J., Durce, D., Salah, S., Cánovas, C.R., Smolders, E., 2023. Remediation of acid mine drainage and immobilization of rare earth elements: comparison between natural and residual alkaline materials. Appl. Geochem. 158, 105800. https://doi.org/10.1016/j.apgeochem.2023.105800.

Kotte-Hewa, D.J., Durce, D., Salah, S., Vantelon, D., Smolders, E., 2024. Association of rare earth elements with secondary mineral phases formed during alkalinization of acid mine drainage. Sci. Total Environ. 948, 174895. https://doi.org/10.1016/j.scitotenv.2024.174895.

León, R., Macías, F., Cánovas, C.R., Pérez-López, R., Ayora, C., Nieto, J.M., Olías, M., 2021. Mine waters as a secondary source of rare earth elements worldwide: the case of the Iberian Pyrite Belt. J. Geochem. Explor. 224, 106742. https://doi.org/10.1016/j.gexplo.2021.106742.

LME, 2023. London metal exchange official prices for metal global market. https://www.lme.com/. June 2023.

Lottermoser, B.G., 2011. Recycling, reuse and rehabilitation of mine wastes. Elements 7, 405–410. https://doi.org/10.2113/gselements.7.6.405.

Lozano, A., Ayora, C., Fernández-Martínez, A., 2019. Sorption of rare earth elements onto basaluminite: the role of sulfate and pH. Geochem. Cosmochim. Acta 258, 50–62. https://doi.org/10.1016/j.gca.2019.05.016.

Macias, F., Caraballo, M.A., Nieto, J.M., Rötting, T.S., Ayora, C., 2012a. Natural pretreatment and passive remediation of highly polluted acid mine drainage. J. Environ. Manag. 104, 93–100. https://doi.org/10.1016/j.jenvman.2012.03.027.

Macías, F., Caraballo, M.A., Rötting, T.S., Pérez-López, R., Nieto, J.M., Ayora, C., 2012b. From highly polluted Zn-rich acid mine drainage to non-metallic waters: implementation of a multi-step alkaline passive treatment system to remediate metal pollution. Sci. Total Environ. 433, 323–330. https://doi.org/10.1016/j.scitotenv.2012.06.084.

Macías, F., Pérez-López, R., Caraballo, M.A., Cánovas, C.R., Nieto, J.M., 2017a. Management strategies and valorization for waste sludge from active treatment of extremely metal-polluted acid mine drainage: a contribution for sustainable mining. J. Clean. Prod. 141, 1057–1066. https://doi.org/10.1016/j.jclepro.2016.09.181.

Macías, F., Pérez-López, R., Caraballo, M.A., Sarmiento, A.M., Cánovas, C.R., Nieto, J.M., et al., 2017b. A geochemical approach to the restoration plans for the Odiel River basin (SW Spain), a watershed deeply polluted by acid mine drainage. Environ. Sci. Pollut. Control Ser. 24, 4506–4516. https://doi.org/10.1007/s11356-016-8169-9.

Marouane, B., Klug, M., As, K.S., Engel, J., Reichel, S., Janneck, E., Peiffer, S., 2021. The potential of granulated schwertmannite adsorbents to remove oxyanions (SeO32−, SeO42−, MoO42−, PO43−, Sb (OH) 6−) from contaminated water. J. Geochem. Explor. 223, 106708. https://doi.org/10.1016/j.gexplo.2020.106708.

Martin, J.D., 2004. Using XPowder: a software package for Powder X-Ray diffraction analysis. DL GR 1001 (4), 105.

Millán-Becerro, R., Cánovas, C.R., Macías, F., Roetting, T.S., Siddorn, L., Stanley, P., Nieto, J.M., 2023. Passive remediation of mine waters from Parys Mountain (Wales): laboratory column experiments. J. Clean. Prod. 425, 138872. https://doi.org/10.1016/j.jclepro.2023.138872.

Moses, C.O., Nordstrom, D.K., Herman, J.S., Mills, A.L., 1987. Aqueous pyrite oxidation by dissolved oxygen and by ferric iron. Geochem. Cosmochim. Acta 51 (6), 1561–1571. https://doi.org/10.1016/0016-7037(87)90337-1.

Mwewa, B., Tadie, M., Ndlovu, S., Simate, G.S., Matinde, E., 2022. Recovery of rare earth elements from acid mine drainage: a review of the extraction methods. J. Environ. Chem. Eng. 10 (3), 107704. https://doi.org/10.1016/j.jece.2022.107704.

Noack, C.W., Dzombak, D.A., Karamalidis, A.K., 2014. Rare earth element distributions and trends in natural waters with a focus on groundwater. Environ. Sci. Technol. 48 (8), 4317–4326.

Nordstrom, D., 1982. Aqueous pyrite oxidation and the consequent formation of secondary iron minerals. Acid Sulfate Weathering 10, 37–56. https://doi.org/10.2136/sssaspecpub10.c3.

Orden, S., Macías, F., Cánovas, C.R., Nieto, J.M., Pérez-López, R., Ayora, C., 2021. Eco-sustainable passive treatment for mine waters: full-scale and long-term demonstration. J. Environ. Manag. 280, 111699. https://doi.org/10.1016/j.jenvman.2020.111699.

Pinedo Vara, I., 1963. Piritas de Huelva. Summa, Madrid, p. 1003.

Rakotonimaro, T.V., Neculita, C.M., Bussière, B., Zagury, G.J., 2016. Effectiveness of various dispersed alkaline substrates for the pre-treatment of ferriferous acid mine drainage. Appl. Geochem. 73, 13–23. https://doi.org/10.1016/j.apgeochem.2016.07.014.

Rakotonimaro, T.V., Neculita, C.M., Bussière, B., Benzaazoua, M., Zagury, G.J., 2017. Recovery and reuse of sludge from active and passive treatment of mine drainage-impacted waters: a review. Environ. Sci. Pollut. Control Ser. 24, 73–91. https://doi.org/10.1007/s11356-016-7733-7.

Sánchez-España, J., Yusta, I., López, G.A., 2012. Schwertmannite to jarosite conversion in the water column of an acidic mine pit lake. Mineral. Mag. 76 (7), 2659–2682. https://doi.org/10.1180/minmag.2012.076.7.03.

Silberglitt, R.S., Silberglitt, R., Bartis, J.T., Chow, B.G., An, D.L., Brady, K., 2013. Critical Materials: Present Danger to US Manufacturing. Rand Corporation. www.rand.org/pubs/research_reports/RR133.

Smith, K.S., Figueroa, L.A., Plumlee, G.S., 2013. Can Treatment and Disposal Costs Be Reduced through Metal Recovery? International Mine Water Association Conference IMWA2013 -Reliable Mine Water Technology (Golden, Colorado), pp. 729–734.

SMM, 2023. Shangai metals market. https://www.metal.com/. June 2023.

Stolpe, B., Guo, L., Shiller, A.M., 2013. Binding and transport of rare earth elements by organic and iron-rich nanocolloids in Alaskan rivers, as revealed by field-flow fractionation and ICP-MS. Geochem. Cosmochim. Acta 106, 446–462. https://doi.org/10.1016/j.gca.2012.12.033.

Tabelin, C.B., Uyama, A., Tomiyama, S., Villacorte-Tabelin, M., Phengsaart, T., Silwamba, M., et al., 2022. Geochemical audit of a historical tailings storage facility

in Japan: acid mine drainage formation, zinc migration and mitigation strategies. J. Hazard Mater. 438, 129453. https://doi.org/10.1016/j.jhazmat.2022.129453.
USGS, 2023. Mineral Commodity Summaries 2023. U.S. Geological Survey, 2023, Mineral Commodity Summaries 2023. U.S. Geological Survey. https://doi.org/10.3133/mcs2023, 2014pp.
Young, P.L., 1997. The longevity of minewater pollution: a basis for decision-making. Sci. Total Environ. 194, 457–466. https://doi.org/10.1016/S0048-9697(96)05383-1.